INSTITUTE OF PHYSICS PUBLISHING INVERSE PROBLEMS

Inverse Problems **18** (2002) 1127–1146 PII: S0266-5611(02)31095-5

Reconstruction of a current distribution from its magnetic field

Rainer Kress, Lars Kühn and Roland Potthast[1]

Institut for Numerical and Applied Mathematics, University of Göttingen, Germany

Received 21 November 2001, in final form 7 May 2002
Published 15 July 2002
Online at stacks.iop.org/IP/18/1127

Abstract

We consider the inverse problem of reconstructing a current distribution from measurements of its magnetic field. Uniqueness issues and simulations for the reconstruction are studied. Given the magnetic field on a surface surrounding the current distribution we show that a projection of the current distribution can be reconstructed uniquely. In addition, we derive some properties of directed current distributions that reflect the properties and difficulties of the reconstruction. A Tikhonov-projection scheme complemented by an artefact-correction algorithm is employed to reconstruct the current distribution within a cuboid. By numerical examples in three dimensions we show that for measurement errors up to 1% we can detect areas of low-current density within the cuboid.

(Some figures in this article are in colour only in the electronic version)

Dedicated to Erich Martensen on the occasion of his 75th birthday.

1. Introduction

Assume that measurements of the magnetic field H produced by a current distribution j in a three-dimensional conducting domain Ω are taken on the surface of a domain containing Ω in its interior. Consider the task of reconstructing the current distribution j within Ω from the measured magnetic field H. In particular, we are interested in the detection of areas within Ω where the conductivity is low and where the currents are small.

We will reconstruct currents j which arise in the form $j = \sigma \operatorname{grad} \varphi$ from an electric potential φ satisfying

$$\operatorname{div} \sigma \operatorname{grad} \varphi = 0 \tag{1.1}$$

in a bounded domain $\Omega \subset \mathbb{R}^3$ and satisfy the boundary condition

$$\nu \cdot \sigma \operatorname{grad} \varphi = g \tag{1.2}$$

[1] http://www.scienceatlas.de/nfg.

0266-5611/02/041127+20$30.00

on the boundary of Ω, where ν denotes the exterior normal vector to $\partial\Omega$. The industrial problem which builds the background of the problem (1.1), (1.2) is the reconstruction of current densities within fuel cells from their magnetic fields. Fuel cells are innovative devices that produce electricity from renewable fuel and there is a huge interest in the monitoring of the internal current distribution in these cells both for research, development and maintenance purposes. With the industrial problem there is also a strong interest in directed currents, since by chemical arguments and technical design the currents in a fuel cell can only flow in one direction. For this reason we will investigate the special situation of the reconstruction of directed currents. We will show that the assumption of directedness has some consequences, but in general does not yield better uniqueness results for the problem as expected by our industrial partners.

However, we think that the results are highly interesting within a wider range of applications. At two points they overlap the field of medical magnetic imaging, where a current density $j = j_e + j_s$ needs to be reconstructed from magnetic measurements where $j_e = \sigma \operatorname{grad} \varphi$ is a solution of the inhomogeneous problem

$$\operatorname{div} \sigma \operatorname{grad} \varphi = \operatorname{div} j_s \tag{1.3}$$

in a domain Ω with a source current j_s and boundary condition

$$\nu \cdot \sigma \operatorname{grad} \varphi = 0 \tag{1.4}$$

on $\partial\Omega$ (see literature cited below). *First*, for biomagnetic problems a current density j needs to be reconstructed from its magnetic field H or from the normal component $\nu \cdot H$ of the magnetic field on some exterior surface. The reconstruction procedure presented in this work will apply to this problem, since it does not need any assumptions on the nature of the currents under consideration. In particular, we analyse the null-space of the Biot–Savart integral operator W that maps the currents j onto their exterior magnetic field H and show that in general at most a projection of the current j can be reconstructed. This applies both to the fuel-cell application and to the biomedical problem. *Second*, we will derive a characterization of the 'realistic' currents for the fuel-cell model, that theoretically analyses the relation between the projected reconstructed currents and the true currents in the cell. We expect this analysis to lead to more involved reconstruction algorithms in the near future. We would like to encourage the biomedical community to derive analogous characterizations for the biomedical model situation (1.3), (1.4).

We first address the topic of *uniqueness* and *characterize* the space of current distributions in terms of the Biot–Savart operator W. Then, we apply a *Tikhonov regularization* to the solution of the ill-posed integral equation of the first kind $Wj = H$. We show that the Tikhonov regularization reconstructs the *projection* of the current distribution onto the orthogonal complement of the nullspace $N(W)$ with respect to an appropriate inner product. Our theoretical analysis is complemented by a *numerical study* of current reconstructions with simulated data in three dimensions. This includes an *artefact-correction algorithm* to deal with artefacts produced by regularization in the case of noisy data.

In order to make our work accessible to a broader audience we include some of the classical results both from the potential theory for static magnetic fields and from the theory of regularization of ill-posed problems.

Before we proceed, we will provide a brief review and discussion of some related work dealing with current reconstructions from magnetic fields. All the following works deal with current reconstruction from magnetic fields, where the underlying model from which the currents arise may differ from application to application.

Banks and Kojima [1] investigated a two-dimensional problem. The direct problem considered in their paper treats a homogeneous conductor using a boundary value problem

for the electric potential. Then, as an inverse problem, they try to detect an interior boundary that encircles a nonconducting area, i.e. an area with vanishing currents. They search for this boundary curve by minimization of a fit-to-data functional.

Sarvas [15] gave a detailed introduction to the physics of biomagnetic imaging, i.e. the visualization of currents inside a body from their magnetic fields. The direct model investigates the currents that arise from electromotive forces impressed by biological activities in conducting tissues. For the direct (and inverse) problem Sarvas considers a piecewise constant conductivity and reduces the problem to a Poisson equation with transmission conditions at the interfaces between the domains of piecewise constant conductivity and with a compactly supported source term in $\mathbb{R}^3$. For the inverse problem Sarvas employs a least-squares fit, notes that numerical instabilities occur, and states the need for regularization.

In principle, Tilg and Wach [17] follow the approach of Sarvas considering currents that arise from biological activities and consider piecewise constant conductivities. For the inverse problem they use a Wiener filter estimation as a regularization method to reconstruct currents on a two-dimensional surface (the outer cortex surface) separating two regions of different conductivities in the human brain. Similar problems reconstructing currents on surfaces in the brain were treated by Ramon and colleagues [11] and [14], both using a least-squares fit. In [11] it is shown that the Biot–Savart operator has a nontrivial nullspace and a projection method is employed to deal with this nonuniqueness. Jeffs *et al* [8] investigate the inversion of the Biot–Savart operator by a singular-value decomposition and algebraic reconstruction technique (ART) that leads to a (weighted) minimum norm solution.

The use of biomagnetic imaging for the location of magnetic sources in cardiomagnetic inverse problems is described, e.g., by Stroink [16]. There is a number of papers on *probabilistic* reconstruction methods for bioelectromagnetic inverse problems, see the literature cited in [17]. Furthermore, we mention the work on the related topic of classical impedance tomography and refer, among many others, to [2, 7].

In our numerical simulations we treat the fuel-cell geometry and consider current distributions in a cuboid with the axis parallel to the coordinate axis. This directly applies to the standard fuel-cell model from industrial applications. The theory, numerical analysis and implementation of the *direct problem* to compute the current distribution within Ω and the magnetic field outside Ω (for given conductivity distributions in Ω and current influxes through the boundary $\partial\Omega$) has been considered in [12]. We follow [12] and use the finite integration technique for the forward model, i.e. we solve a discretized version of the knot equation $\operatorname{div} j = 0$ and the equation $\operatorname{curl} j = 0$ on a grid. As shown in [12], this method has linear convergence when the grid size tends to zero. For the discretization of the Biot–Savart integral operator W and solution of the *inverse problem* we will use a straightforward rectangular rule for the calculation of the integrals, which also leads to linear convergence for the forward problem.

2. The uniqueness problem for current reconstructions

This section is concerned with the uniqueness question for the reconstruction of current distributions from the measurement of the magnetic field on some surface containing the conducting domain Ω in its interior.

2.1. The magnetic field in the exterior domain

First, we consider a magnetic field H defined in the exterior $\Omega_e := \mathbb{R}^3 \backslash \overline{\Omega}$ of some simply connected bounded domain $\Omega \subset \mathbb{R}^3$. For the *inverse* problem treated later we will measure

the trace of this magnetic field on the boundary ∂G of some domain G with $\overline{\Omega} \subset G$ or parts of this boundary only. Therefore we need to investigate whether these measurements uniquely determine the magnetic field in Ω_e. This will be done using a boundary value problem in the exterior of G. In particular, by theorem 1 we will answer the question under which assumptions the normal component $\nu \cdot H$ determines the magnetic field and when the full trace of H on the exterior surface is necessary. For the fuel-cell application we will show that knowledge of the normal component is not sufficient for determining H, but that the measurement of the full field H is sufficient, see theorem 2.

We base our analysis on the static *Maxwell equations*

$$\begin{aligned} &\operatorname{curl} H = j, \quad \operatorname{curl} E = 0, \\ &\operatorname{div} D = \rho, \quad \operatorname{div} B = 0 \end{aligned} \tag{2.1}$$

and the *material equations*

$$D = \epsilon E, \qquad B = \mu H, \qquad j = \sigma E \tag{2.2}$$

where ϵ and μ are constants and where we assume that the conductivity σ is inhomogeneous and anisotropic, i.e. σ is a matrix function. In particular, we assume that there are no currents in the exterior Ω_e of Ω and that the current satisfies

$$\operatorname{div} j = 0 \qquad \text{in } \Omega \tag{2.3}$$

and

$$\nu \cdot j = 0 \qquad \text{on } \partial\Omega, \tag{2.4}$$

where ν denotes the outward unit normal of $\partial\Omega$. Condition (2.3) is a consequence of the vector identity div curl $= 0$ and the Maxwell equation $\operatorname{curl} H = j$. Condition (2.4) implies that there is no current flux through $\partial\Omega$. Our main argument for the introduction of this condition is the search for an appropriate assumption under which the normal component of H is sufficient for determining H in the exterior Ω_e of Ω. For the fuel-cell application condition (2.4) is *not* satisfied and we will provide an adequate result for this case below.

If both conditions (2.3) and (2.4) are fulfilled H is given by Biot–Savart's law

$$H(x) = \operatorname{curl} \int_\Omega \Phi(x, y)\, j(y)\, \mathrm{d}s(y), \qquad x \in \Omega_e, \tag{2.5}$$

and satisfies $\operatorname{curl} H = 0$ in Ω_e, see [10, 12]. Here, as in [12], we use the notation

$$\Phi(x, y) := \frac{1}{4\pi |x - y|}, \qquad x \neq y \in \mathbb{R}^3,$$

for the fundamental solution of the Laplace equation in $\mathbb{R}^3$.

Since Ω_e is simply connected, $\operatorname{curl} H = 0$ implies that H can be expressed as a gradient field, i.e. in the exterior Ω_e of Ω we have

$$H = \operatorname{grad} \varphi_H \tag{2.6}$$

with a magnetic potential φ_H. From equations (2.1) and (2.6) and the identity div grad $= \Delta$ we observe that the magnetic potential φ_H satisfies the Laplace equation

$$\Delta \varphi_H = 0 \qquad \text{in } \Omega_e. \tag{2.7}$$

We will measure either the magnetic field H on the boundary ∂G or only its normal component $\nu \cdot H$ with the outward unit normal ν of ∂G. In the latter case we are given the normal derivative

$$\frac{\partial \varphi_H}{\partial \nu} = g \qquad \text{on } \partial G \tag{2.8}$$

of the potential φ_H, where we denote the measured normal component of H by g. Since the potential is determined only up to a constant, we normalize φ_H by the condition

$$\varphi_H(x) = o(1), \qquad |x| \to \infty, \tag{2.9}$$

uniformly for all directions. Then, the magnetic potential φ_H satisfies an exterior Neumann problem for the Laplace equation in the unbounded domain $G_e := \mathbb{R}^3 \backslash G$ as defined by (2.7)–(2.9).

The well known uniqueness and existence results on this classical potential theoretic boundary value problem can be summarized as follows. The exterior Neumann problem (2.7)–(2.9) for the Laplace equation is uniquely solvable. For a proof we refer to [9], theorems 6.11 and 6.24. Since solutions to the Laplace equation are analytic in their domain of definition (see [9]), from the uniqueness in G_e we conclude that the magnetic potential φ_H is uniquely determined in all of Ω_e through the normal derivative on ∂G. Consequently we can state the following theorem.

Theorem 1. *Let H be the magnetic field generated through Biot–Savart's law (2.5) by a current distribution j in Ω that satisfies conditions (2.3) and (2.4). Then H is uniquely determined in all of Ω_e by the normal components $\nu \cdot H$ of H on ∂G.*

For modelling the fuel-cell problem it is necessary to consider nonclosed systems and allow current distributions j in Biot–Savart's law (2.5) that do not satisfy the flux condition (2.4). In this case, H as given by (2.5) no longer satisfies $\operatorname{curl} H = 0$ in Ω_e and therefore the above arguments do not apply. However, as a derivative of a volume potential H satisfies the vector Laplace equation in Ω_e, i.e. its Cartesian components satisfy the Laplace equation. Now we can apply the uniqueness for the exterior Dirichlet problem for the Laplace equation in G_e (see [9], theorem 6.11), i.e. the maximum–minimum principle for harmonic functions, and again the analyticity of solutions to the Laplace equation to establish the following theorem.

Theorem 2. *Let H be the magnetic field generated through Biot–Savart's law (2.5) by a current distribution j in Ω that does not necessarily satisfy the conditions (2.3) and (2.4). Then H is uniquely determined in all of Ω_e by the trace of H on ∂G.*

2.2. Nonuniqueness and nullspaces

As the next step we show that in general there is no uniqueness for the reconstruction of current distributions from their magnetic fields, i.e. the Biot–Savart operator $W : C(\bar{\Omega}) \to C(\partial G)$ defined by

$$(Wj)(x) = \operatorname{curl} \int_\Omega \Phi(x, y) j(y) \, \mathrm{d}y, \qquad x \in \partial G, \tag{2.10}$$

has a nontrivial nullspace.

Later, we will relate this nullspace to the realistic solution space of current densities. Here, the term realistic is attached to currents that arise within the fuel-cell model (1.1), (1.2).

Definition 3. *We call a current distribution j* realistic *if it satisfies* $\operatorname{div} j = 0$ *in Ω and is based on a conductivity distribution σ in the sense of Ohm's law*

$$j = \sigma E \tag{2.11}$$

with the electric field $E \in (C(\bar{\Omega}))^3 \cap (C^1(\Omega))^3$ satisfying the static Maxwell equations $\operatorname{div} E = 0$, $\operatorname{curl} E = 0$ *in Ω. For this we assume that the conductivity is described by a positive definite matrix function $\sigma : \Omega \to \mathbb{R}^3 \times \mathbb{R}^3$.*

We note that curl $E = 0$ in Ω implies the existence of an electric potential φ_E such that $E = \operatorname{grad} \varphi_E$. The above properties of a realistic current distribution imply that, after an appropriate normalization, φ_E is a solution to the interior Neumann problem

$$\operatorname{div} \sigma \operatorname{grad} \varphi_E = 0 \qquad \text{in } \Omega, \tag{2.12}$$

$$\nu \cdot \sigma \operatorname{grad} \varphi_E = g \qquad \text{on } \partial\Omega, \tag{2.13}$$

$$\int_\Omega \varphi_E \, \mathrm{d}s = 0 \tag{2.14}$$

with some function $g \in C(\partial\Omega)$ satisfying $\int_{\partial\Omega} g \, \mathrm{d}s = 0$. This elliptic boundary value problem is investigated in section 2.2 of [12]. In particular, the set of realistic current distributions is a linear subspace of $(H^1(\Omega))^3$.

We denote the space of two-times continuously differentiable vector fields $\Omega \to \mathbb{R}^3$ with compact support in Ω by $(C_0^2(\Omega))^3$. The following theorem will enable us to construct a large set of nontrivial current densities in Ω that have a vanishing magnetic field in the exterior of Ω. This set is as large as the space $(C_0^2(\Omega))^3$ itself and basically describes the nullspace of the operator W.

Theorem 4. *The nullspace*

$$N(W) = \{j \in (C(\Omega))^3 : Wj = 0 \text{ on } \partial G\} \tag{2.15}$$

of the operator $W : C(\Omega) \to C(\partial G)$ contains the linear subspace

$$M := \{j = \Delta m : m \in (C_0^2(\Omega))^3\}. \tag{2.16}$$

Proof. For $j \in M$ there exists $m \in (C_0^2(\Omega))^3$ such that $j = \Delta m$. Then, from Green's second integral theorem we have that

$$\begin{aligned}\int_\Omega \Phi(x, y) j(y) \, \mathrm{d}y &= \int_\Omega \Phi(x, y) \Delta m(y) \, \mathrm{d}y \\ &= \int_\Omega \Delta_y \Phi(x, y) m(y) \, \mathrm{d}y + \int_{\partial\Omega} \left\{ \Phi(x, y) \frac{\partial m}{\partial \nu}(y) - m(y) \frac{\partial \Phi(x, y)}{\partial \nu(y)} \right\} \mathrm{d}s(y)\end{aligned}$$

for $x \in \Omega_e$. The right-hand side vanishes, since $\Delta \Phi(x, \cdot) = 0$ in Ω for $x \in \Omega_e$ and m vanishes together with its derivative on the boundary $\partial\Omega$. This implies that

$$\int_\Omega \Phi(x, y) j(y) \, \mathrm{d}y = 0$$

for $x \in \Omega_e$ and the proof is finished. □

We note that by imposing the condition $\operatorname{div} m = 0$ in Ω we obtain current distributions that fulfil the conditions (2.3) and (2.4).

2.3. Properties of directed current densities

Since by the previous theorem, in general, we do not have uniqueness for the reconstruction of current distributions from their magnetic fields, we will now investigate the question whether this uniqueness can be restored by restricting ourselves to directed current distributions. As mentioned in the introduction, directed currents arise in fuel cells, where the chemical process and design of the cell allows only one direction of electron flow. We will see that for directed current distributions in general we will *not* obtain uniqueness, but we can show that nontrivial directed current distributions will always produce nontrivial magnetic fields.

Definition 5. *We call a current distribution* $j \in (C(\bar{\Omega}))^3$ directed *if there exists a* direction $d \in \mathbb{R}^3$ *with* $|d| = 1$ *such that*

$$j(x) \cdot d \geqslant 0, \qquad x \in \Omega. \tag{2.17}$$

Furthermore, we call a directed current distribution j cone directed *if for some angle* $0 < \beta < \pi/2$ *we have*

$$j(x) \cdot d \geqslant \tan\beta |j(x)| \tag{2.18}$$

for all $x \in \Omega$.

Then from theorem 2 we can deduce the following result.

Theorem 6. *Let* $j \in (C(\bar{\Omega}))^3$ *be a cone directed current distribution that does not necessarily fulfil conditions (2.3) and (2.4) and let the magnetic field* H *induced by* j *through Biot–Savart's law (2.5) satisfy* $H = 0$ *on* ∂G. *Then we have* $j = 0$ *in* Ω.

Proof. We choose the coordinate system such that the x_3-axis coincides with the vector d and Ω is part of the upper half space. According to Biot–Savart's law we have

$$H(x) = \frac{1}{4\pi} \int_\Omega \frac{j(y)(x-y)}{|x-y|^3}\, \mathrm{d}y, \qquad x \in \Omega_e.$$

Consequently the second component H_2 of H is given by

$$H_2(x) = \frac{1}{4\pi} \int_\Omega \frac{j_3(y)(x_1 - y_1) - j_1(y)(x_3 - y_3)}{|x-y|^3}\, \mathrm{d}y \tag{2.19}$$

for all points of the form $x = (x_1, 0, x_3)$. Since j is a cone-directed distribution, with a constant $\tilde{\beta} := \tan(\beta)$ we have the estimates

$$j_3(y) \geqslant \tilde{\beta} |j_1(y)|, \qquad y \in \Omega, \tag{2.20}$$

and

$$j_3(y) \geqslant \tilde{\beta} |j_2(y)|, \qquad y \in \Omega. \tag{2.21}$$

Since Ω is a bounded set there is a constant R such that $|y| < R$ for $y \in \Omega$. For

$$x_1 > \tilde{\beta} R + R \tag{2.22}$$

we now obtain

$$\tilde{\beta} y_3 - (x_1 - y_1) < 0.$$

For $x_3 = 0$ and x_1 chosen so that (2.22) is satisfied we obtain

$$\begin{aligned} j_3(y)(x_1 - y_1) - j_1(y)(x_3 - y_3) &= -j_1(y) y_3 - j_3(y)(x_1 - y_1) \\ &\geqslant (\tilde{\beta} y_3 - (x_1 - y_1)) j_3(y) \geqslant 0, \end{aligned} \tag{2.23}$$

where equality can only occur when $j_3(y) = 0$. In this case from (2.20) we conclude that $j_1(y) = 0$. From (2.19) and (2.23) we find that

$$H_2(x) \geqslant 0,$$

and thus, for sufficiently large x_1, we have proven the equivalence

$$H_2(x_1, 0, 0) = 0 \qquad \text{if and only if } j_1 = j_3 = 0 \qquad \text{in } \Omega. \tag{2.24}$$

Since by theorem 2 the condition $H = 0$ on ∂G implies that $H = 0$ in the exterior of Ω from the equivalence (2.24) we conclude that $j_1 = j_3 = 0$ in Ω.

With the same arguments applied to the components H_1, j_2 and j_3 and a point $x = (0, x_2, 0)$ with $x_2 > \tilde{\beta} R + R$ we obtain that $j_2 = j_3 = 0$ in Ω, i.e. $j = 0$ in Ω, and the proof is complete. □

We proceed with a result on the reconstruction of a directed current distribution with direction $d = (0, 0, 1)$ in a rectangular domain $\Omega_\square$ given by

$$\Omega_\square = \left\{ y = (y_1, y_2, y_3) \in \mathbb{R}^3 : |y_1| < \frac{a_1}{2},\ |y_2| < \frac{a_2}{2},\ |y_3| < \frac{a_3}{2} \right\} \tag{2.25}$$

with parameters $a_j > 0$, $j = 1, 2, 3$. We denote the vertical part of the boundary $\partial\Omega_\square$ by $\tilde{\Gamma}$, i.e.,

$$\tilde{\Gamma} := \left\{ y = (y_1, y_2, y_3) \in \partial\Omega_\square : |y_3| < \frac{a_3}{2} \right\}$$

and assume that condition (2.4) is satisfied only on $\tilde{\Gamma}$, i.e.,

$$\nu \cdot j = 0 \qquad \text{on } \tilde{\Gamma}. \tag{2.26}$$

Theorem 7. *Let j be a realistic and directed current distribution in $\Omega_\square$ with direction $d = (0, 0, 1)$ satisfying (2.26) that is based on a positive definite conductivity distribution σ. Assume that the magnetic field H induced by j through Biot–Savart's law (2.5) satisfies $H = 0$ on ∂G. Then $j = 0$ in $\Omega_\square$.*

Proof. As a continuous function the component j_1 is bounded on $\Omega_\square$. Therefore we can estimate

$$\left| \int_{\Omega_\square} \frac{j_1(y) y_3}{|x - y|^3} \, \mathrm{d}y \right| \leqslant \frac{c_1}{|x|^3} \tag{2.27}$$

for all sufficiently large values of $|x|$ and some constant c_1. Since by assumption $j_3(y) \geqslant 0$ for all $y \in \Omega_\square$, we have $j_3(y)(x_1 - y_1) \geqslant 0$ for all sufficiently large x_1 and $y \in \Omega_\square$. Assume that $j_3 \neq 0$. Then we obtain

$$\left| \int_{\Omega_\square} \frac{j_3(y)(x_1 - y_1)}{|x - y|^3} \, \mathrm{d}y \right| \geqslant \frac{c_2}{|x_1|^2} \tag{2.28}$$

for all sufficiently large $x = (x_1, 0, 0)$ and some positive constant c_2. This yields

$$|H_2(x)| \geqslant \frac{c}{|x_1|^2} \tag{2.29}$$

for all sufficiently large $x = (x_1, 0, 0)$ and some positive constant c, where H_2 is given by (2.19). On the other hand, by theorem 2 from $H = 0$ on ∂G we have that $H = 0$ in $\mathbb{R}^3 \backslash \Omega_\square$. This contradicts (2.29) and consequently $j_3 = 0$ in $\Omega_\square$. Together with (2.26) this implies that $\nu \cdot j = 0$ on $\partial\Omega_\square$.

From this, since we assume that in $\Omega_\square$ we have $\operatorname{div} j = 0$ and $j = \sigma E$ with $E = \operatorname{grad} \varphi_E$, using the Gauss divergence theorem we can conclude that

$$\int_{\Omega_\square} E \cdot \sigma E \, \mathrm{d}x = \int_{\Omega_\square} \operatorname{grad} \varphi_E \cdot j \, \mathrm{d}x = \int_{\partial\Omega_\square} \varphi_E \nu \cdot j \, \mathrm{d}s = 0.$$

Finally, this implies $E = 0$ in $\Omega_\square$, since σ is positive definite and consequently $j = \sigma E = 0$ in $\Omega_\square$. □

Remark. In general the results of theorems 6 and 7 do *not* yield uniqueness for reconstructions of current densities. The difference of two directed current densities does not need to be directed and then we have no results on this difference. Moreover, adding a small element of the nullspace of W to a directed current distribution will produce another directed current distribution with the same exterior magnetic field. Geometrically, the results show that for the set E of cone directed current distributions and the nullspace $N(W)$ in the space $(C(\bar{\Omega}))^3$ the relation

$$N(W) \cap E = \{0\}, \tag{2.30}$$

is satisfied, i.e. the nullspace of W and the set E have only the trivial function in common.

2.4. Characterization of the solution space

As a further step after the investigation of directed current distributions we now derive a characterization of the targeted solution space of the inverse problem in terms of the nullspace of the Biot–Savart operator W. To this end we need to take into account the conductivity σ, which will be unknown in the end, but is an integral part of the analysis of the inverse problem. Given a matrix function $\sigma : \Omega \to \mathbb{R}^3 \times \mathbb{R}^3$ we define the space $(L^2_\sigma(\Omega))^3$ as the set $(L^2(\Omega))^3$ equipped with the inner product

$$\langle \varphi, \psi \rangle_\sigma := \int_\Omega \varphi(y) \cdot \sigma(y)^{-1} \overline{\psi(y)} \, \mathrm{d}y, \qquad \varphi, \psi \in (L^2(\Omega))^3. \tag{2.31}$$

Here, we assume that $\sigma(y)$ is boundedly invertible for all $y \in \Omega$, i.e.

$$\max\{||\sigma(y)||_\infty, ||\sigma^{-1}(y)||_\infty\} \leqslant C_\sigma \tag{2.32}$$

for all $y \in \Omega$ and some constant C_σ. Looking from a set-theoretic point of view, the space $(L^2_\sigma(\Omega))^3$ is identical to the classical space $(L^2(\Omega))^3$. But the inner product in $(L^2_\sigma(\Omega))^3$ has a different orthogonality which will be crucial for the characterization of the correct current density. For a subset $U \subset (L^2(\Omega))^3$ we define

$$U^{\perp_\sigma} := \{\varphi \in (L^2(\Omega))^3 : \langle \varphi, \psi \rangle_\sigma = 0 \text{ for all } \psi \in U\}. \tag{2.33}$$

We initially need to do some preparations in the spirit of potential theory, see, e.g., Martensen [10], p 45.

Lemma 8. *Let $j \in (C^1(\Omega))^3 \cap (C(\bar{\Omega}))^3$ be a current distribution satisfying* div $j = 0$ *in* Ω. *Then we have*

$$\text{curl } Wj = j - \text{ grad } S(\nu \cdot j) \qquad \text{in } \Omega \tag{2.34}$$

with the single-layer operator

$$(Sg)(x) := \int_{\partial\Omega} \Phi(x, y) g(y) \, \mathrm{d}s(y), \qquad x \in \Omega.$$

Proof. We introduce the vector potential

$$(Vj)(x) = \int_\Omega \Phi(x, y) j(y) \, \mathrm{d}s(y), \qquad x \in \Omega.$$

Then, using the vector identity curl curl $= -\Delta +$ grad div and $\Delta Vj = -j$ in Ω for the volume potential (see [3], theorem 8.1) we obtain that

$$\text{curl } Wj = \text{ curl curl } Vj = j + \text{ grad div } Vj.$$

With the aid of div $j = 0$ and the Gauss divergence theorem we transform

$$\int_\Omega \text{div}_x(\Phi(x, y) j(y)) \, \mathrm{d}y = -\int_\Omega \text{div}_y(\Phi(x, y) j(y)) \, \mathrm{d}y = \int_{\partial\Omega} \Phi(x, y) \nu(y) \cdot j(y) \, \mathrm{d}s(y)$$

for x in Ω, i.e., putting the two previous equations together we have shown (2.34). □

For the rest of this section we assume that σ and its inverse are symmetric, i.e.

$$\sigma^T = \sigma, \qquad (\sigma^{-1})^T = \sigma^{-1}.$$

On the space

$$X := \{j \in (H^1(\Omega))^3 : \text{div } j = 0\}$$

we define the operator S^∇ by

$$(S^\nabla l)(x) := (\text{ grad } S(\nu \cdot j))(x), \qquad x \in \Omega,$$

where $\nu \cdot j$ is defined on the boundary $\partial\Omega$ of Ω. In terms of S^∇ we set

$$\mathcal{N} := (I - S^\nabla) N(W)$$

and are now in a position to prove the following characterization theorem.

Theorem 9. *Let j be a realistic current distribution based on a conductivity distribution σ. Then j is orthogonal to $\mathcal{N}$ with respect to the orthogonality in $L^2_\sigma(\Omega)$, i.e.*

$$j \in \mathcal{N}^{\perp_\sigma}. \tag{2.35}$$

Proof. For $\tilde{m} \in \mathcal{N}$ there is $m \in N(W)$ such that $\tilde{m} = m - \operatorname{grad} S(\nu \cdot m)$. For convenience we abbreviate $m_\nu = \nu \cdot m|_{\partial\Omega}$. Then using lemma 8, the vector identity

$$\operatorname{div}(a \times b) = b \cdot \operatorname{curl} a - a \cdot \operatorname{curl} b$$

and $\operatorname{curl} \sigma^{-1} j = \operatorname{curl} \operatorname{grad} \varphi_E = 0$ we transform

$$\langle j, \tilde{m} \rangle_\sigma = \langle j, m - \operatorname{grad} S m_\nu \rangle_\sigma = \int_\Omega j \cdot \sigma^{-1} \overline{(m - \operatorname{grad} S m_\nu)}\, \mathrm{d}y = \int_\Omega \sigma^{-1} j \cdot \overline{\operatorname{curl} W m}\, \mathrm{d}y$$
$$= \int_\Omega \operatorname{div}\left(\overline{W m} \times \sigma^{-1} j\right) \mathrm{d}y = \int_{\partial\Omega} \nu \cdot \left(\overline{W m} \times \sigma^{-1} j\right) \mathrm{d}s.$$

From this, in view of $Wm = 0$, the statement of the theorem follows. □

3. A Tikhonov-projection algorithm for the inverse problem

This section is devoted to the use of the Tikhonov regularization for the reconstruction of a current distribution from its magnetic fields using the Biot–Savart operator (2.10). In particular, we need to address the lack of uniqueness as investigated in section 2. Instead of reconstructing the original currents, we will show that the Tikhonov regularization reconstructs a *projection* of these currents onto some subspace of $(L^2(\Omega))^3$.

The Tikhonov regularization describes a stable method for the solution of ill-posed operator equations

$$A\varphi = f \tag{3.1}$$

in a Hilbert space setting, i.e., the operator A is a linear and compact operator from a Hilbert space X into a Hilbert space Y. For an introduction to the theory of ill-posed problems and regularization methods we refer to [3, 4, 9]. Since the paper attempts to address a broader audience we will summarize the relevant results and then describe the special problems due to nonuniqueness of the Biot–Savart operator W.

The background for the solution of (3.1) by Tikhonov regularization is given by the singular value decomposition and Picard's theorem. Let (μ_n, φ_n, g_n) be a singular system of the operator A, i.e., (μ_n) is the set of non-negative square roots of the eigenvalues of the self-adjoint operator $A^*A : X \to X$, where $A^* : Y \to X$ is the adjoint of A. Please note that the eigenvalues of a self-adjoint compact operator $A^*A \neq 0$ form a countable set in $\mathbb{R}$ accumulating only at zero. The vectors φ_n and g_n are defined as in the following theorem. For a proof we refer to theorem 4.7 in [3].

Theorem 10 (Singular value decomposition). *Let (μ_n) be the sequence of non-negative singular values of the compact linear operator $A \neq 0$, ordered such that*

$$\mu_1 \geqslant \mu_2 \geqslant \mu_3 \geqslant \cdots \tag{3.2}$$

with repetitions according to the multiplicity of the singular value, i.e., according to the dimension of the nullspace $N(\mu_n^2 I - A^*A)$. Then there exist orthonormal vectors (φ_n) in X and (g_n) in Y such that

$$A\varphi_n = \mu_n g_n, \qquad A^* g_n = \mu_n \varphi_n \tag{3.3}$$

for all $n \in \mathbb{N}$. For each $\varphi \in X$ we have the singular value decomposition

$$\varphi = \sum_{n=1}^{\infty} (\varphi, \varphi_n)\varphi_n + Q\varphi \tag{3.4}$$

with the orthogonal projection operator $Q : X \to N(A)$ and

$$A\varphi = \sum_{n=1}^{\infty} \mu_n (\varphi, \varphi_n) g_n. \tag{3.5}$$

Each system (μ_n, φ_n, g_n) of this type is called a singular system of A.

The solution of (3.1) is based on the following theorem. For a proof we refer to theorem 4.8 in [3].

Theorem 11 (Picard). *Let $A : X \to Y$ be a compact linear operator with singular system (μ_n, φ_n, g_n). Then equation (3.1) is solvable if and only if $f \in N(A^*)^{\perp}$ and*

$$\sum_{n=1}^{\infty} \frac{1}{\mu_n^2} |(f, g_n)|^2 < \infty. \tag{3.6}$$

In this case a solution to (3.1) is given by

$$\varphi = \sum_{n=1}^{\infty} \frac{1}{\mu_n} (f, g_n)\varphi_n. \tag{3.7}$$

Picard's theorem illustrates the ill-posedness of the Biot–Savart equation $Wj = H$. As noted already, $(\mu_n)_{n\in\mathbb{N}}$ accumulates only at zero. Thus, the values $1/\mu_n$ tend to infinity for $n \to \infty$, and small errors in the data are strongly enlarged.

If the operator A is *not* injective, the projection operator Q in the representation (3.4) is nonzero. Arbitrary elements ψ of the nullspace $N(A)$ may be added to the solution of equation (3.1) without changing the right-hand side, i.e., if we are given $\psi \in N(A)$ and a solution φ of (3.1), then the function $\varphi + \psi$ is a solution and a unique reconstruction of φ is not possible. But we can reconstruct a special projection of the solution using Tikhonov regularization as follows. For a proof see theorem 4.13 in [3].

Theorem 12 (Tikhonov regularization). *Let A be a compact linear operator. Then for each $\alpha > 0$ the operator $\alpha I + A^*A : X \to X$ is bijective and has a bounded inverse. We call $\varphi_\alpha := R_\alpha f$ with the operator*

$$R_\alpha := (\alpha I + A^*A)^{-1} A^* \tag{3.8}$$

the Tikhonov solution of (3.1) with regularization parameter α in the spaces X and Y. If A is injective and φ satisfies $A\varphi = f$, then we have

$$\varphi_\alpha \to \varphi, \qquad \alpha \to 0. \tag{3.9}$$

If A is not injective, the operator R_α is an operator onto the space $N(A)^{\perp}$. This is a consequence of the property

$$A^*Y \subset N(A)^{\perp} \tag{3.10}$$

(see Picard's theorem) which implies that $\alpha I + A^*A$ maps the space $N(A)^{\perp}$ onto itself. Let φ be a solution of

$$A\varphi = f. \tag{3.11}$$

Then according to the regularization property (3.9) of the Tikhonov regularization applied in the subspace $N(A)^{\perp}$, the function $\varphi_\alpha = R_\alpha f$ defines an approximation for the orthogonal projection $\varphi_0 := P\varphi$ of φ on $N(A)^{\perp}$ and we have proven the *convergence*

$$\varphi_\alpha \to P\varphi, \qquad \alpha \to 0. \tag{3.12}$$

In this context we also refer to Groetsch [6].

Finally, we remark that in general, according to (2.35) and section 2.4 for the reconstruction of current densities j, the true current density depends on σ and is *not* an element of $N(A)^{\perp}$ with $A = W$.

4. A numerical study using the grid model and artefact correction

For the numerical solution of the inverse problem of current reconstruction a programme package in MATLAB has been developed. The purpose of this section is summarized in the following points.

(1) The main routine uses a 'measured' magnetic field H and a regularization parameter α as input. It calculates a *projection* onto $N(W)^{\perp}$ of the original current distribution via the Tikhonov regularization (3.8) applied to the equation $Wj = H$.
(2) The results give numerical evidence that the location of low-current areas (the blue spots in the density plots of this section) can be detected from this projection of the original density distribution. This is a nontrivial observation, since the Tikhonov regularization only reconstructs a projection of the original function and this projection could lead to significant changes in the location of low-current areas.
(3) For selected examples we have calculated the norm difference of the original and the reconstructed density, but since we do not expect convergence, we restrict our attention to qualitative demonstration of the location of low- and strong-current areas in the reconstructions as shown in the images.
(4) We show how numerical artefacts introduced by the systematic error of the Tikhonov regularization may be treated using some new *artefact-correction algorithm*. The results give numerical evidence that this method significantly improves the reconstructions.
(5) We demonstrate the influence of different grid sizes on the ill-posedness of the reconstruction.

Remark. In general the use of the same grid both for simulations and reconstructions for some inverse problem is known as *inverse crime* (cf [3]). Working on some fixed grid, the ill-posedness of the inverse problem is significantly reduced as compared with the full continuous problem. We use the easier problem for fixed grids to demonstrate its severe ill-posedness and to introduce the artefact correction. As a second step the difficulty with different grids is treated at the end of the section.

In the following, we will present the typical results for reconstructions. The goal is to explore the practical possibilities of reconstructions for current densities using the Tikhonov-projection algorithm. The Biot–Savart operator is discretized by the rectangular rule on a regular grid in the cuboid Ω and a regular grid on the surface of some cylinder containing Ω. Thus, for the numerics the operator W is represented by some matrix $\boldsymbol{W}$ to which the Tikhonov equation is applied.

First, we show a rough estimate for the computing times solving the linear system by MATLAB. We used a Compaq Professional Workstation XP 1000 (1280 MB main memory) with True64 UNIX V4.0F. For grids up to the size $[9, 9, 9] \equiv 2187$ points we used 2400 measurement points. Then we added more measurement points such that the number of available data slightly exceeded the number of unknowns.

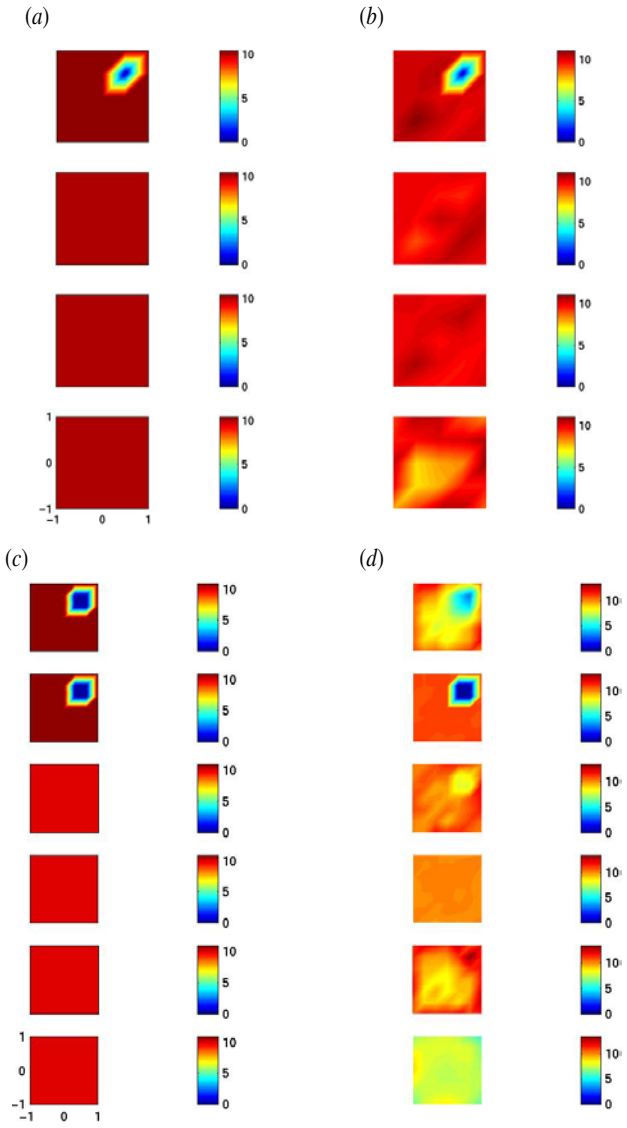

Figure 1. True current distribution (*a*) and reconstruction with 1% data error and a regularization parameter $\alpha = 10^{-2}$ on a [5, 5, 5]-grid ((*b*), same on a [7, 7, 7]-grid ((*c*), (*d*)). The blue colour indicates areas of low currents (arising from underlying defects in the fuel-cell application), the red and yellow areas show large current densities. (Colour key in online version only.)

Grid size	Number of measurements	Time for reconstruction
[5, 5, 5]	$3 \times 20 \times 40 = 2400$	25 s
[7, 7, 7]	$3 \times 20 \times 40 = 2400$	120 s (2 min)
[9, 9, 9]	$3 \times 20 \times 40 = 2400$	410 s (5 min)
[11, 11, 11]	$3 \times 30 \times 50 = 4500$	2600 s (45 min)
[13, 13, 13]	$3 \times 40 \times 55 = 6600$	—

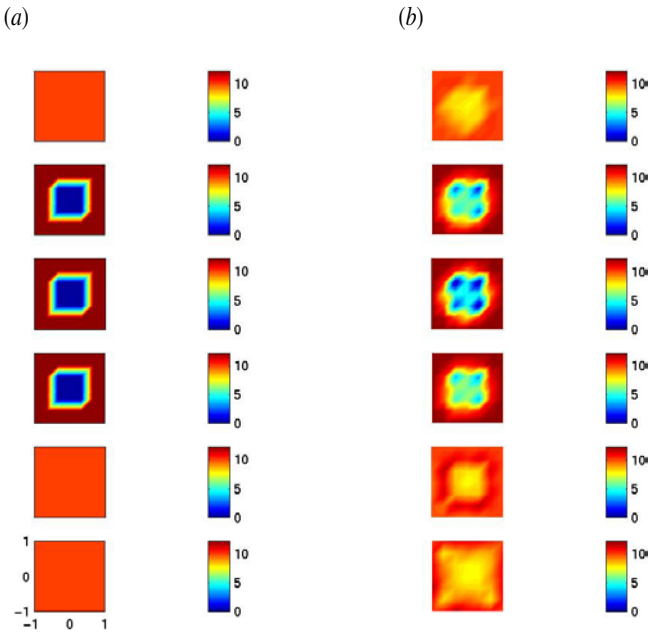

Figure 2. True current distribution (*a*) and reconstruction with exact data and a regularization parameter $\alpha = 10^{-11}$ (*b*). (Colour key in online version only.)

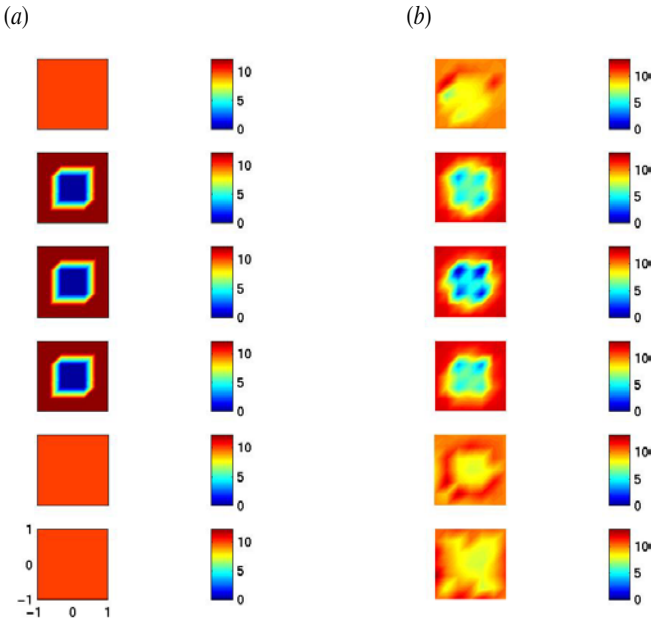

Figure 3. True current distribution (*a*) and reconstruction with data error 10^{-6} and a regularization parameter $\alpha = 10^{-11}$ (*b*). (Colour key in online version only.)

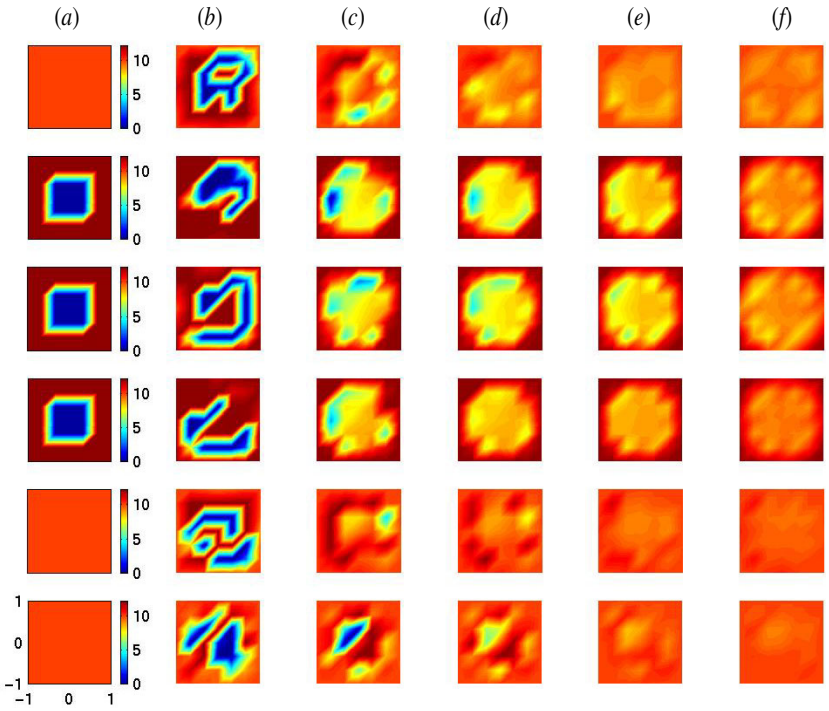

Figure 4. True current distribution (a) and reconstruction with data error $d = 10^{-4}$ (a) and regularization parameters $\alpha = 10^{-11}$ (b), 10^{-8} (c), 10^{-7} (d), 10^{-6} (e), 10^{-5} (f). If the regularization parameter is chosen too small, then we obtain the typical artefacts shown in (b), where the values of the reconstructed current density show huge variations which are produced by the data error and the instability of the inverse problem. If the regularization parameter becomes larger, the smoothing and regularization error takes control over the influence of the data error and we obtain blurred images. (Colour key in online version only.)

Figure 1 demonstrates an example of a reconstruction on a [5, 5, 5]-grid (upper images) with an error of 1% and the regularization parameter $\alpha = 10^{-2}$. The left-hand column shows the true current densities in the x_3-direction, the right-hand column the reconstructed current densities. In the lower images we calculated on a [7, 7, 7]-grid, where the area of low-current density is the effect of low conductivity defined by some function in $\mathbb{R}^3$ independent of the grid size and sampled at the grid points.

The relative error of the reconstruction in figure 1 is 0.1361 using the Frobenius norm

$$||J|| := \left(\sum_{klm} (J^2_{klmx_1} + J^2_{klmx_2} + J^2_{klmx_3}) \right)^{1/2}, \tag{4.1}$$

i.e. approximately 13%. If we calculate the error of the x_3-component only, we obtain the even better value of 0.0635, i.e. about 6%. The relative errors of the x_3-component are much smaller than the relative errors of the x_1- and x_2-components. This is reasonable since we measure the magnetic field only on the shell of the cylinder and not on the base and the top.

Next, we present a series of more complex reconstructions that demonstrate the difficulty of reconstruction and visualization of variations of the current density in the interior of the cuboid. First, we produced the current density illustrated by figure 2(a) on a grid with seven discretization points in each direction. Figure 2(b) shows a reconstruction with perfect data on the original [7, 7, 7]-grid. The measurements have been taken at 800 points on

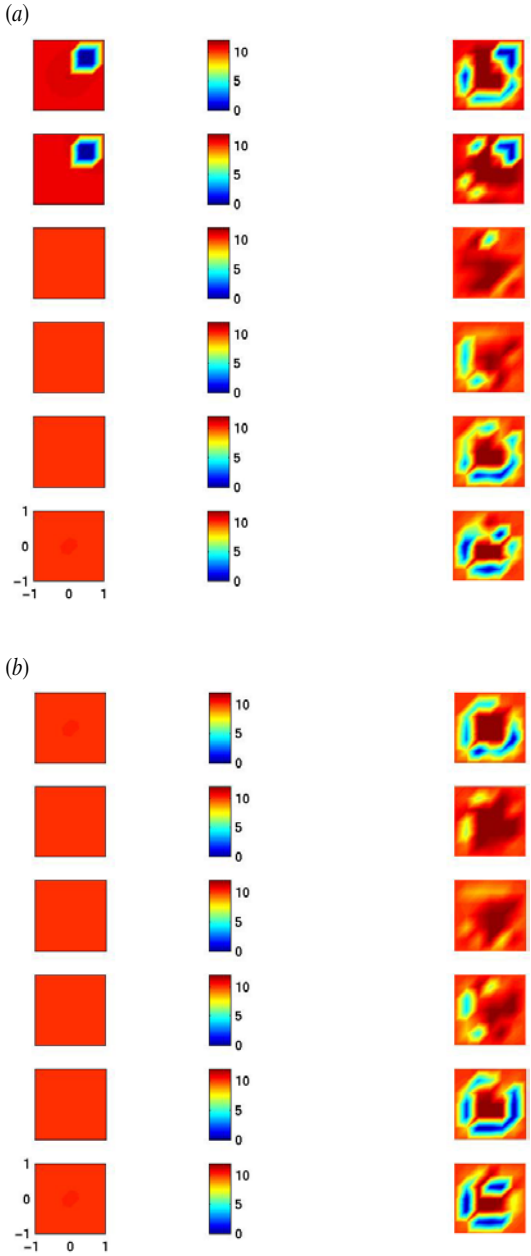

Figure 5. (*a*) A reconstruction with $d = 10^{-4}$ and regularization parameter $\alpha = 10^{-8}$ on a [7, 7, 7]-grid with central current input. We obtain strong artefacts in the upper and lower part of the cuboid. However, the same artefacts appear when reconstructing the currents for a homogeneous conductivity distribution (*b*). (Colour key in online version only.)

the cylinder surface (20 circles with 40 points each), i.e. the matrix $\boldsymbol{W}$ had the dimension $2400 \times 1029 = 2469\,600$. We show variations of the data error d and the regularization parameter α.

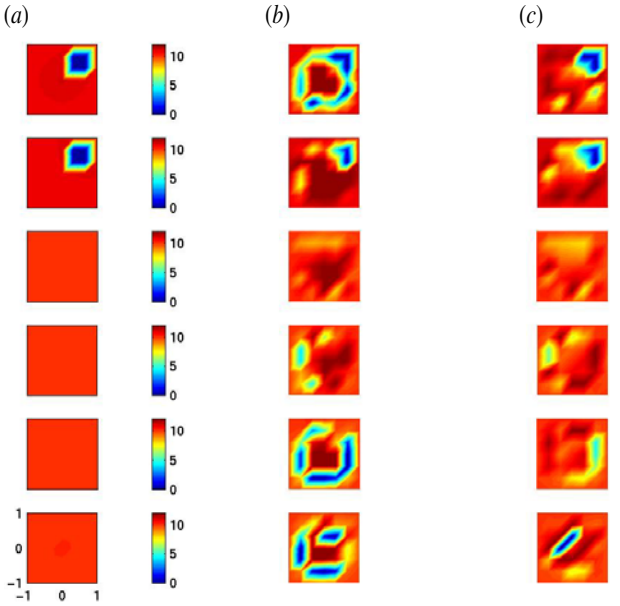

Figure 6. True current distribution on a [7, 7, 7]-grid with centred current input (*a*) and reconstruction with $d = 10^{-4}$ and regularization parameter $\alpha = 10^{-8}$ without correction (*b*) and with correction (*c*). (Colour key in online version only.)

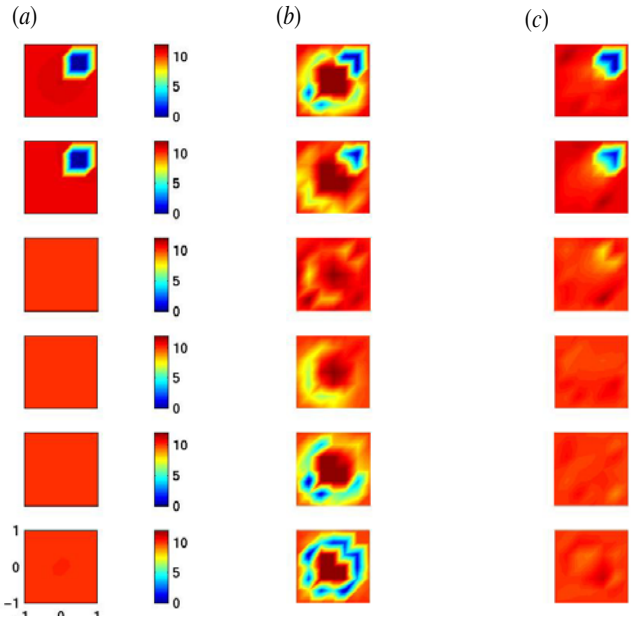

Figure 7. True current distribution on a [7, 7, 7]-grid with centred current input (*a*) and reconstruction with $d = 10^{-4}$ and regularization parameter $\alpha = 10^{-6}$ without correction (*b*) and with correction (*c*). (Colour key in online version only.)

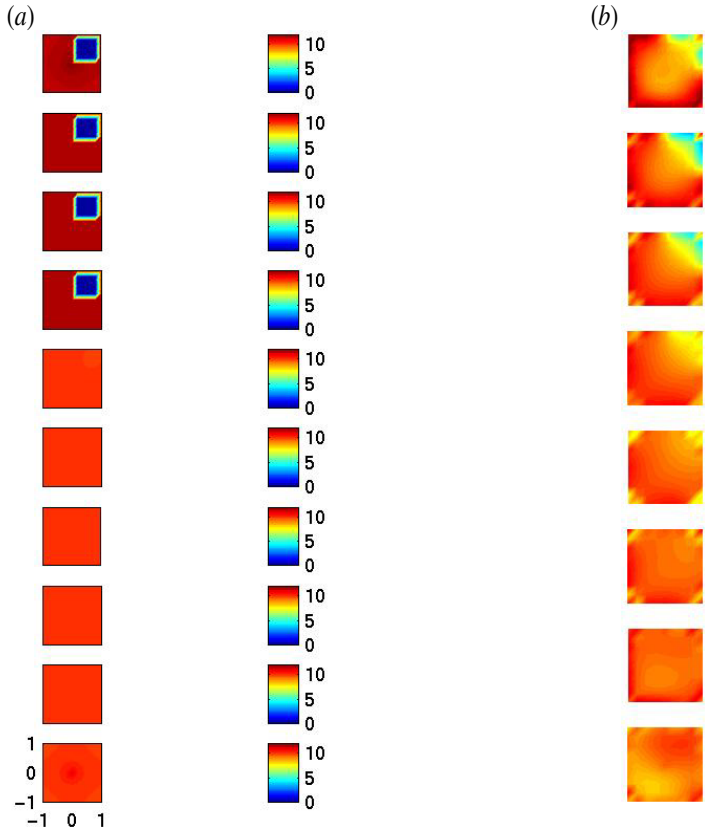

Figure 8. Reconstruction on a [9, 9, 9]-grid with data error $d = 10^{-2}$ and a regularization parameter $\alpha = 10^{-2}$ (*b*) from a magnetic field produced by the current distribution on a [11, 11, 11]-grid (*a*). The image demonstrates that reconstructions on a grid different from the grid used for the forward simulation are even more ill-posed than the reconstruction on the grid used for the forward model. (Colour key in online version only.)

Now, we successively add a larger data error to the magnetic field, keeping α as it is. Up to an error of size $d = 10^{-6}$ we obtain reasonable reconstructions showing the low-current area, as illustrated in figure 3.

At a data error of size $d = 10^{-4}$ the reconstruction breaks down and we obtain the behaviour shown in figure 4. In figure 4(*f*) with $\alpha = 10^{-5}$ the smoothing of the regularization is sufficiently large enough to correct the errors produced by the data error. But this smoothing degrades the reconstruction and the areas of low-current density blur as shown by the image.

4.1. Central current input

For all previous examples we used a homogeneous current input at the base of the cuboid and a homogeneous outflow at the top. Now, we study the case where the current input is performed at a single point in the centre of the base and the full current flows out at the centre of the top surface of the cuboid. This will cause further difficulties, as shown by figure 5, which shows an image analogous to figure 1. We obtain strong artefacts in the upper and lower areas of the cuboid.

The artefacts are caused by the regularization error and are not produced by data errors, as proven by figure 5(*b*). This leads to the following artefact-correction scheme which we demonstrate in figure 6. Figure 6(*b*) shows the Tikhonov scheme without correction. Figure 6(*c*) demonstrates the results of the correction scheme. Even better results are obtained for the regularization parameter $\alpha = 10^{-6}$, see figure 7.

To eliminate the artefacts we used the following *artefact-correction algorithm*. We could obtain significant improvements in the reconstructions and image quality.

(1) Use the Tikhonov-projection scheme to calculate the reconstructed current density J_{rek} on the grid $\mathcal{G}$.
(2) For the grid $\mathcal{G}$ and a constant conductivity distribution calculate the corresponding current density J_0 and its magnetic field H_0 using the solution of the forward problem (1.1), (1.2) and the Biot–Savart operator W.
(3) Use the Tikhonov-projection scheme to reconstruct the density J_0 from its magnetic field H_0. This yields a vector of reconstructed currents $J_{0,rek}$. Since this density should coincide with J_0, all differences are identified as 'artefacts'. Calculate

$$J_\delta := J_0 - J_{0,rek}. \tag{4.2}$$

(4) Now, we correct the original reconstructed current density using J_δ, i.e. we calculate

$$J_{corr} := J_{rek} + J_\delta. \tag{4.3}$$

To quantify the improvement provided by the artefact correction we calculated the relative error for the reconstructions shown in figures 6 and 7.

	Relative error	
	Pure Tikhonov	Tikhonov plus artefact correction
Figure 6	0.5856	0.1813
Figure 7	0.5387	0.0508

4.2. Reconstructions with different grid sizes

Finally, we need to study the reconstruction of a current density when the grid size is not known or when the magnetic field is produced by some fine grid (approximating a continuous current distribution) and reconstructions are performed on a coarse grid.

We calculated the magnetic fields for current distributions on grids of the size [11, 11, 11] and studied the reconstructions on a coarser grid. An example is shown in figure 8. Here, we need to point out that the wrong choice of the regularization parameter will produce useless pictures as in figure 4 (where we obtain huge artefacts or where the image is fully blurred).

References

[1] Banks H T and Kojima F 2000 Boundary shape identification in two-dimensional electrostatic problems using SQUIDs *J. Inverse Ill-Posed Problems* **5** 487–504
[2] Cheney M, Isaacson D and Newell J 1999 Electrical impedance tomography *SIAM Rev.* **41** 85–101
[3] Colton D and Kress R 1998 *Inverse Acoustic and Electromagnetic Scattering Theory* 2nd edn (Berlin: Springer)
[4] Engl H W, Hanke M and Neubauer A 1996 *Regularization of Inverse Problems* (Dordrecht: Kluwer)
[5] Gerthsen Ch, Kneser H O and Vogel H 1974 *Physik* (Berlin: Springer)
[6] Groetsch C W 1984 *The Theory of Tikhonov Regularization for Fredholm Equations of the First Kind* (Boston, MA: Pitman)

[7] Hanke M 1996 *Mathematische Grundlagen der Impedanztomographie* Lecture, University of Karlsruhe
[8] Jeffs B, Leahy R and Singh M 1987 An evaluation of methods for neuromagnetic image reconstruction *IEEE Trans. Biomed. Eng.* **34** 713–23
[9] Kress R 1999 *Linear Integral Equations* 2nd edn (Berlin: Springer)
[10] Martensen E 1968 *Potentialtheorie* (Stuttgart: Teubner)
[11] Ok S, Ramon C, Marks R J, Nelson A C and Meyer M G 1993 Resolution enhancement of biomagnetic images using the method of alternating protections *IEEE Trans. Biomed. Eng.* **40** 323–8
[12] Potthast R and Kühn L 2002 On the convergence of the finite integration technique for the anisotropic boundary value problem of magnetic impedance tomograph *Math. Methods Appl. Sci.* at press
[13] Potthast R, Kühn L, Vogt A and Hauer K-H 2001 *Rekonstruktion Einer Stromdichteverteilung aus den von ihr Erzeugten Magnetfeldern für das Monitoring von Brennstoffzellen* (Göttingen: Projektreport)
[14] Ramon C, Meyer M G, Nelson A C, Spelman F A and Lamping J 1993 Simulation studies of biomagnetic computed tomography *IEEE Trans. Biomed. Eng.* **40** 317–22
[15] Sarvas J 1987 Basic mathematical and electromagnetic concepts of the biomagnetic inverse problem *Phys. Med. Biol.* **32** 11–22
[16] Stroink G 1993 *Cardiomagnetic Imaging in Frontiers in Cardiovascular Imaging* ed B L Zaret, L Kaufman, A S Berson and R A Dunn (New York: Raven)
[17] Tilg B and Wach P 1995 An iterative approach on magnetic source imaging within the human cortex—a simulation study *Int. J. Biomed. Comput.* **40** 51–7